Astronomy & Astrophysics manuscript no.
(will be inserted by hand later)

The Distance Scale of Planetary Nebulae

T. Bensby and I. Lundström

Lund Observatory, Box 43, S-22100 Lund, Sweden

Received / Accepted

Abstract. By collecting distances from the literature, a set of 73 planetary nebulae with mean distances of high accuracy is derived. This sample is used for recalibration of the mass-radius relationship, used by many statistical distance methods. An attempt to correct for a statistical peculiarity, where errors in the distances influences the mass–radius relationship by increasing its slope, has been made for the first time. Distances to PNe in the Galactic Bulge, derived by this new method as well as other statistical methods from the last decade, are then used for the evaluation of these methods as distance indicators. In order of achieving a Bulge sample that is free from outliers we derive new criteria for Bulge membership. These criteria are much more stringent than those used hitherto, in the sense that they also discriminate against background objects. By splitting our Bulge sample in two, one with optically thick (small) PNe and one with optically thin (large) PNe, we find that our calibration is of higher accuracy than most other calibrations. Differences between the two subsamples, we believe, are due to the incompleteness of the Bulge sample, as well as the dominance of optical diameters in the "thin" sample and radio diameters in the "thick" sample.
Our final conclusion is that statistical methods give distances that are at least as accurate as the ones obtained from many individual methods. Also, the 'long' distance scale of Galactic PNe is confirmed.

Key words. planetary nebulae: general

1. Introduction

Planetary nebulae (PNe), being formed at the end of the asymptotic giant branch (AGB), constitute a short but important phase in the evolution of low and intermediate mass stars. Potentially, they can be used as probes of the distribution and kinematics of both their progenitors, i.e. AGB stars, and their end products, i.e. white dwarfs. The PNe show a strong concentration towards the Galactic Centre (GC). Among the $\sim$ 1500 known PNe, more than 25% are located in the direction of the Galactic Bulge (from here on only referred to as 'the Bulge'). The great majority of these are most probably situated within the Bulge, and they are interesting as targets both as individual objects and for statistical treatment.

A major obstacle in most investigations of PNe is the lack of accurate distance determinations. A large collection of so called 'statistical' distance determination methods have been proposed, each using only a few observational properties and using more or less well founded assumptions on the mean values of other parameters needed, such as the mass of the ionized nebular envelope and the filling factor.

All of these methods are in some way related to the method by Shklovsky (1956), in which the main assumptions are that all PNe are optically thin spheres of constant density and have the same nebular mass. Given the large variations in morphology and other observable parameters among PNe, it is not very likely that these assumptions are representative for most PNe. Usually, modifications to the original method involve changes of one or more of the assumptions above. An often used modification has been to replace the assumption of a constant ionized mass with a correlation of the nebular mass with observable quantities.

In a recent paper by Ciardullo et al. (1999), a comparison between distances obtained through the method of identification of resolved binary companions of PNe nuclei and several statistical distance scales is made. Their results suggest that practically all statistical methods gives distances that are too large, except for older ones such as the method by Daub (1982). Newer distance scales that in general are longer have therefore been put into question.

In this paper we will investigate the question of the accuracy of the statistical methods, and if they produce distances that are reliable enough. We will start by discussing the major statistical distance methods that have been proposed during the last decade, Sect. 2, and point on the weaknesses these methods contain. Sect. 3 is then

Send offprint requests to: T. Bensby,
e-mail: thomas@astro.lu.se

devoted to the problem of achieving a sample of PNe with individually determined distances that can be used for calibration of the mass-radius method, which is carried out in Sect. 4. In Sect. 5 we define new criteria for Bulge PNe that not only weed out foreground objects, but background objects as well. Sect. 6 then analyzes the validity of our method and the effects of our criteria for Bulge membership. Finally in Sect. 7 we give some concluding remarks.

2. Previous distance scales

In the original Shklovsky method one assumes that all PNe can be approximated by spheres of fully ionized (or 'density bounded') hydrogen with a constant mass and a uniform density. The expansion of the nebula is then reflected by a synchronous decrease in the density of the emitting gas. If the nebula is optically thin at radio wavelengths, its distance, in parsecs, can be shown to be (see e.g. Milne & Aller, 1975)

$$D = \left[\frac{2.58 \cdot 10^{20} M_{\rm ion}^2 \ln(9980\, t^{3/2})}{\varepsilon\, t^{1/2}\, \theta^3\, S_{5\,\rm GHZ}} \psi \right]^{1/5}, \qquad (1)$$

where θ is the angular diameter of the nebula in seconds of arc, ε is the filling factor, $M_{\rm ion}$ is the ionized nebular mass in solar masses, $t = T_{\rm e}/10^4$ K is the electron temperature, and $S_{5\,\rm GHz}$ is the free-free continuum radio flux at the 5 GHz frequency given in Jansky[1]. ψ is a term involving the singly and doubly ionized helium contribution and is given by

$$\psi = \left[\frac{(1 + y + x''y)(1 + y + 2.7x''y)}{(1 + 4y)^2} \right], \qquad (2)$$

where y is the number abundance ratio of helium to hydrogen ($= N_{\rm He}/N_{\rm H}$) and x'' is the fraction of doubly ionized helium atoms ($= N_{\rm He^{++}}/N_{\rm He}$). Adopting the following values for some of the parameters: $y = 0.11$, $x'' = 0.5$ and $T_{\rm e} = 10\,000$ K, Eq. (1) reduces to

$$D = 17\,580\, M_{\rm ion}^{2/5} \varepsilon^{-1/5} \theta^{-3/5} S_{5\,\rm GHz}^{-1/5}. \qquad (3)$$

Usually, a constant value (normally $\sim 0.5 - 0.6$) has been adopted for the filling factor. In order to avoid the assumption of a constant mass in the equation above, different authors have tried to find relations between either the masses, the surface brightness temperatures or the optical thicknesses and the radii of the nebulae. No matter what, in the end all distance scales end up with distances that are dependent of only two parameters: the 6 cm radio flux and the angular size, as measured from either optical or radio wavelengths. During the last decade several such distance scales have been proposed, notably Cahn, Kaler and Stanghellini (1992) (hereafter CKS), Van de Steene and Zijlstra (1995) (VdSZ), Zhang (1995) (Z95), and Schneider and Buckley (1996) (SB96).

[1] 1 Jy $= 10^{-26}$ Wm^{-2}Hz^{-1}

CKS: Daub (1982) empirically related the nebular ionized mass to a thickness parameter $\mathcal{T}$ defined by

$$\mathcal{T} = \log\left(\frac{\theta^2}{S_{5\,\rm GHz}} \right). \qquad (4)$$

CKS then recalibrated Daub's distance scale using a selection of 19 PNe with well-known distances. Their new relationship was split in two, one for optically thick PNe ($\mathcal{T} < 3.13$) and a constant value for optically thin PNe ($\mathcal{T} > 3.13$), resulting in distances given by

$$\log D = \begin{cases} 2.71 + 0.2\log\theta - 0.6\log S, & \mathcal{T} < 3.13 \\ 3.96 - 0.6\log\theta - 0.2\log S, & \mathcal{T} > 3.13. \end{cases} \qquad (5)$$

For the distance determination CKS used radio fluxes and optical diameters except for nebulae with very small angular sizes, where radio diameters obtained with VLA were used.
The main source of uncertainty is the small number of PNe used in the calibration. The two different relations for thin and thick nebulae are also not very well determined.

VdSZ: This method is based on a relationship between the distance-independent radio continuum brightness temperature given by

$$T_{\rm b} = 73200 \frac{S_{5\,\rm GHz}}{\theta^2} \qquad (6)$$

and the distance-dependent radius of the nebula, calibrated by a sample of 131 PNe in the Bulge, assuming they all lie at a distance of 8.0 kpc. The criteria used for Bulge membership were: $|l| < 10°$, $|b| < 10°$, $\theta < 20''$, and $S_{5\,\rm GHz} < 100$ mJy. Distances obtained by this method are given by

$$\log D = 3.40 - 0.3\log\theta - 0.35\log S_{5\,\rm GHz}. \qquad (7)$$

A worry is the way calibration nebulae were selected. Foreground nebulae are reasonably well weeded out by the selection criteria used, but no attempts have been made to sort out background objects from the Bulge sample.

Z95: This method uses two correlations: one between the ionized mass and the radius, and one between the radio continuum surface brightness temperature and the radius. The distance scale proposed is an average of the two distances obtained using the correlations, and is given by

$$\log D_{\rm f} = 3.39 - 0.27\log\theta - 0.36\log S_{5\,\rm GHz}. \qquad (8)$$

The correlations were calibrated by 132 PNe with individual distances from Zhang (1993).
One could argue that a possible weakness of this relation is that it is based on only one particular method for determining individual distances.

SB96: This method is based on a relationship between the PN radius and the radio surface brightness. The nebular surface brightness, in Jy/arcsec^2, is given by

$$I = \frac{4\,S_{5\,\mathrm{GHz}}}{\pi\theta^2}, \quad (9)$$

which is a distance-independent quantity. The best-fit relationship between the two parameters results in distances given by

$$\log D = 3.37 - \log\theta - 0.026(\log I)^2 - 0.46\log I. \quad (10)$$

This method differs from the previous ones in the sense that a second order polynomial is used in the calibration. To a large extent their calibrating sample consisted of Bulge PNe for which standard selection criteria (same as VdSZ) were used.

A first concern is the accuracy of the angular diameters used. Stasińska et al. (1991) and Pottasch and Zijlstra (1992) take opposite views regarding the accuracy of optical versus radio measurements of the angular diameters. SB96 also comments that "the situation regarding the angular measurements of PNs is in a sorry state".

Secondly, the selection of a calibrating sample of PNe is not trivial. Usually, nebulae with "good" individual distance determinations are chosen, and such samples often include a large fraction of nearby nebulae. The definition of what constitutes a good distance determination is far from obvious. Alternatively, Bulge nebulae are used and in this case the selection of true members can be troublesome, as well as large errors in the observed parameters, notably the angular sizes.

Finally, there seem to exist a statistical peculiarity in the mass–radius relation that hitherto not has been payed attention to. Errors in the distances have the inevitable effect of increasing the slope of the observed distribution (see Sect. 4.2).

For these reasons we found it worthwhile to reanalyze the problem, paying special attention to the problems discussed above.

3. The calibration sample

3.1. Individual distances

There are many different non-statistical methods for distance determinations of PNe or their central stars, e.g. from identification of a resolved binary companion, from expansion velocities, determination of surface gravities and luminosities etc. For a few PNe trigonometric parallaxes from ground-based measurements or from the Hipparcos mission are available. We have conducted a search through the literature for PNe with individually determined distances. It is important that the distance estimates are independent. Sometimes this might be an awkward thing to objectively decide upon. For example, the extinction maps produced by Lucke (1978) have been used by many authors in order to estimate the amount of reddening towards a nebula. Should these distance estimates be treated as independent or not? Since the methods for interpolating and estimating the extinction differs between different authors, often with widely varying results, we believe that it is all right to do so.

A total of 285 PNe were found from papers spanning three decades in publication dates. For a PN to be qualified as a potential "standard" PN we demanded that it should have at least three independent individual distance determinations. This leaves us with 105 PNe. For these PNe we calculated a mean distance (D) and the error of this mean (ΔD) (computed as the standard deviation divided by the square root of the number of individual distance determinations). All PNe with $\Delta D/D > 0.2$ were then rejected, leaving 41 PNe to work with. We call these selected PNe 'sample A' and they are listed in Table A in the Appendix.

In order to increase the size of our sample we subsequently looked at those PNe with only two individual distance determinations. We selected those that had $\Delta D/D < 0.2$ (ΔD is in this case just the difference between the two distances divided by 2). We call these 32 PNe 'sample B', and they are listed in Table B in the Appendix. A majority of these PNe comes from the paper of Zhang (1993), and as can be seen they are located at larger distances than the PNe in sample A. This also means that the relative errors in observable quantities, especially the angular diameters, generally are larger than for sample A. In the subsequent analysis, the nebulae in this second sample are given the weight 0.5 compared to those in sample A.

3.2. Radio fluxes

Radio fluxes for PNe have been obtained both through single dish and interferometric observations. Zijlstra et al. (1989) noted a systematic difference between their VLA observations at 5 GHz and the corresponding measurements in the Parkes survey (Milne and Aller, 1982), which they suggested to be primarily due to contamination from nearby sources in the single dish observations. For strong sources the difference was attributed to extended halos, which could be missed in the VLA measurements due to lack of sufficiently short baselines.

However, Tylenda et al. (1992) argue, through a comparison of optical and radio determinations of extinction constants, that some of the VLA fluxes, in particular those of Gathier et al. (1983b), Pottasch et al. (1988), and Zijlstra et al. (1989) seem to be systematically too low. Pottasch and Zijlstra (1994) subsequently remeasured a subsample of these sources at lower resolution and found that for faint (< 10 mJy) sources the old VLA fluxes were sometimes too low, but no discrepancies were found for brighter sources.

Most of the PNe observed at 5 GHz by Milne and Aller (1975) and Milne (1979) were also observed at 14.7 GHz (Milne and Aller, 1982). They concluded that most

PNe were optically thin at both frequencies. The smaller 14.7 GHz beam will make these observations less susceptible to contamination. In this investigation we have used the mean flux densities of the Parkes survey at 5 and/or 14.7 GHz and different VLA observations. The 14.7 GHz observations were converted to 5 GHz using the relation $S_\nu \propto \nu^{-0.1}$, i.e. assuming the sources to be optically thin at these wavelengths. References to the observations used are listed in Table C in the Appendix.

The differences between the converted 14.7 GHz fluxes and the observed 5 GHz fluxes were generally found to be small ($< 10\%$ of the mean flux) except for a few faint sources (< 10 mJy), indicating that almost all nebulae are in fact optically thin at both frequencies. There are, however, two nebulae that are optically thick at both 5 and 14.7 GHz, viz. Vy 2-2 and Hb 12 (Purton et al., 1982; Seaquist and Davis, 1983; Aaquist and Kwok, 1991). For these nebulae, we have calculated the flux densities expected at 5 GHz if the nebulae had been optically thin from the observations at higher frequencies presented by these authors.

3.3. Angular diameters

As stated in Sect. 2, angular diameters are, for numerous reasons, not always easy to determine. Firstly, only very few PNe are truly spherical, and some have indeed very irregular shapes. Secondly, many nebulae show extended low intensity halos and/or multiple shell structures and several largely different values for the diameter of a particular nebula are often found in the literature. Thirdly, for small nebulae seeing, tracking errors etc. limit the accuracy that can be obtained. Moreover, the angular size is depending on the wavelength region observed, e.g. [OIII] diameters are usually smaller than those measured in Hα. In radio determinations of angular diameters, several different methods are used (see e.g. Zijlstra et al., 1989), and as will be further discussed in Sect. 5, sometimes optical and radio measurements show large discrepancies.

Ideally, the angular sizes of all PNe should be measured in a consistent way. In radio observations, one often use the 10% contour level of the peak flux density. This method, however, can only be used for bright and well resolved nebulae. Moreover, a rather large fraction of the flux could fall outside this limit, and a lower level might be preferred. However, inspection of published data and images from the HST data archive show that the flux usually drops very fast between contour levels in the interval 15 to 5%, so the choice of level is not very critical.

In this investigation we have in most cases adopted angular diameters for the calibration nebulae from the Strasbourg-ESO Catalogue (SECAT), Acker et al. (1992), (rejecting all PNe that have uncertainty flags and/or upper/lower limit values), after checking with sky survey plates and in many cases with images from the HST Data archive. These checks have in some cases led to significant revisions of the diameters. On HST images, diameters have been determined from the contour at $\sim$5% of peak intensity. For elongated nebulae the mean of the major and minor axis has been used. For references to the sources of the adopted diameters, see Table C in the Appendix.

4. Calibration of the distance method

4.1. Mass - radius relationship

From Eq. (3) we define an 'effective' mass as

$$M_{\rm eff} \equiv \frac{M_{\rm ion}}{\varepsilon^{1/2}} = 2.44 \cdot 10^{-11} D^{5/2} \cdot \theta^{3/2} \cdot S_{5\,\rm GHz}^{1/2}. \quad (11)$$

For an ideal PNe ($\varepsilon = 1$), this effective mass is identical to the usual ionized mass. The filling factor only corrects for (by increasing the mass) that the emitting gas volume is smaller than the one that is obtained by measuring the angular size (which otherwise would result in a too low density).

The PNe radii, in parsecs, are given by

$$R = \tan\left(\frac{\theta/2}{206265}\right) \cdot D \simeq \frac{\theta/2}{206265} \cdot D. \quad (12)$$

Fig. 1a shows the effective masses versus the sizes of the PNe in the two samples (A and B). There are no doubts that the masses keep rising for all radii.

A linear relationship,

$$\log M_{\rm eff} = \alpha \cdot \log R + \beta, \quad (13)$$

is then fitted by weighted least square regression. The constants α and β are derived by minimizing the chi-square merit function (see for instance Press et al. (1997))

$$\chi^2(\alpha,\beta) = \sum_{i=1}^{N} \left(\frac{(\log M_{\rm eff})_i - \alpha - \beta \cdot (\log R)_i}{\sigma_i} \right)^2, \quad (14)$$

where σ_i is the uncertainty associated with each $\log M_{\rm eff}$, i.e. 2.5 times the uncertainty in the distance. Distance uncertainties in sample B, that are given less weight compared to sample A, are also multiplied by a factor two. An approximation here is that we assume the radii to be known exactly (which is not true since errors in the distances translates to the radii as well, although not as much as for the masses). The resulting regression line is given by

$$\alpha = 1.32 \pm 0.04, \quad \beta = 0.55 \pm 0.05. \quad (15)$$

and is plotted as a dotted line in Fig. 1a.

The correlation coefficient of the fit is 0.90 and the standard deviation of the residuals of $\log M_{\rm eff}$ is 0.25. We also tried out other fits to the data: non-weighted fits and second order fits, of which none gave any improved solution.

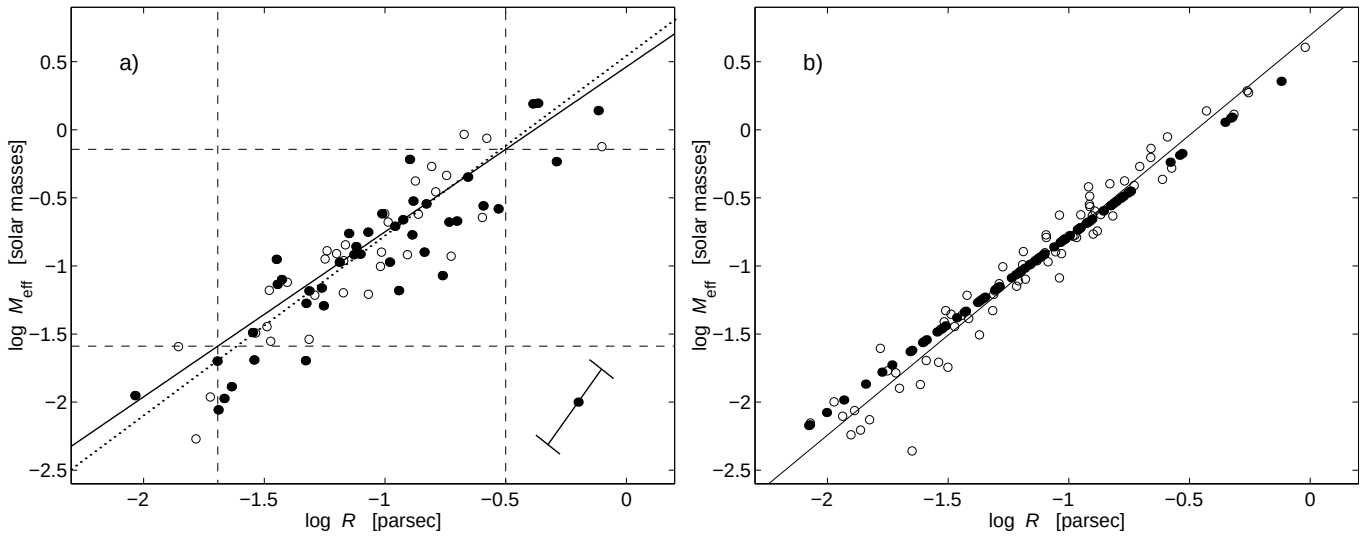

Fig. 1. a) Effective masses versus radii for the calibration samples. Filled circles represent those 41 PNe that have three or more independent distance determinations, open circles those with just two. Two regression lines are also plotted: the original weighted one (dotted line, see Eq. (15)) and the one corrected for uncertainties in the adopted distances (solid line, see Eq. (16)). The error bar indicates how a data point is affected by an uncertainty of 25% in the adopted distances. Dashed lines are explained in Sect. 5.1.
Fig. 1. b) A simulated sequence of PNe lying perfectly along the mass-radius relationship (filled circles). Open circles show how the distribution is steepened when random errors of 30% in the distances are introduced. A regression line is also plotted.

4.2. Corrections to the fit

How do errors in the adopted distances of our calibration sample affect the mass–radius relationship? The error bar in Fig. 1a shows the displacement a data point will undergo for an error of 25% . As can be seen, this 'error vector' ($\log M_{\rm eff}$ is proportional to $2.5 \log D$ and therefore also to $2.5 \log R$) is roughly aligned with the derived regression line, only slightly steeper. A consequence of this, that was pointed out by our referee Dr. A. Zijlstra, is that the observed distribution is steeper than it would be if the distances were error free. Our derived regression coefficients are then too large.

To correct for this effect we will simulate a sequence of PNe lying along our derived relationship. By introducing random errors in the distances of these PNe, and fitting a new linear relationship we will be able to see how large the steepening is. The effect will of course be more prominent the larger the errors in the distances are. From the fit above we saw that the residuals are about 0.25 (in $\log M_{\rm eff}$, i.e. vertically aligned). If the spread's only source is inaccurate distances, this corresponds to a shift of about 0.57 along the error vector back to to regression line. Then an uncertainty of about 70% in the distances of our calibration sample is implied. However, there are errors coupled to the angular sizes and the radio fluxes as well. Then we have different assumptions about the electron temperature, degree of ionization, the geometry of the nebulae etc. Also, the reasoning above is based on the fact that there exists an absolute relationship between the masses and the radii for the nebulae. If not, there is also a kind of intrinsic "cosmic" scatter included in the plot. Therefore, maybe we can assume that the adopted distances are responsible for about 50% of the spread, i.e. ~ 0.12 in the residuals of $\log M_{\rm eff}$. Although this assumption is somewhat precarious, it implies an accuracy of about 30% in the adopted distances.

Fig. 1b shows a sample of 73 PNe (filled circles) lying perfectly along a mass-radius relationship. Empty circles show how random errors in the distances (Gaussian distribution with a σ of 30%) affects the distribution. From the fitting of a regression line to this distribution we see that the slope is increased by 9% and the constant term by 18% (computed as the average from hundreds of simulations, the one shown in the figure is just one representive case).

Compensating the coefficients in Eq. (15) for this effect (i.e. dividing α and β by 1.09 and 1.18 respectively) gives the final relationship (shown as the solid line in Fig. 1a)

$$\log M_{\rm eff} = 1.21 \cdot \log R + 0.46. \qquad (16)$$

One striking thing that can be seen in Fig. 1b is how the down-dip on the lower left, seen in the original data, is reproduced by introducing errors to the distances. This indicates that it might be a kind of artifact and warrants the use of a linear mass-radius relationship.

4.3. Resulting method

By invoking the effective mass-radius relationship from Eq. (13) in Eq. (11), and making use of Eq. (12) it is easy

to show that the distances (in parsecs) are given by

$$\log D = \frac{5.61\alpha - \beta - 10.61}{\alpha - 2.5} + \frac{1.5 - \alpha}{\alpha - 2.5}\log\theta + \frac{0.5}{\alpha - 2.5}\log S_{5\,\mathrm{GHz}}, \quad (17)$$

which through the result of the fit, Eq. (16), becomes

$$\log D = 3.31 - 0.22\,\log\theta - 0.39\,\log S_{5\,\mathrm{GHz}}. \quad (18)$$

This distance relation is really not that different from the ones by VdSZ and Z95. A trend is quite obvious though; our method is less dependent on the angular size, but slightly more on the radio flux, and the zero point is lower. The differences are slightly smaller compared to Z95 than compared to VdSZ. Consequences due to these differences are analyzed in Sect. 6.3.

5. Bulge PNe

5.1. Selection criteria

For a PN to qualify as a member of the Galactic Bulge, it must have certain properties. First of all it must be located in the right direction. The most widely used criteria for the galactic coordinates are $|l| < 10^\circ$ and $|b| < 10^\circ$. At a distance of 8 kpc it corresponds to a Bulge radius of about 1.5 kpc. Further limitations on the nebulae are set upon their angular diameters ($\theta < 20''$) and their 6 cm radio continuum flux ($S_{5\,\mathrm{GHz}} < 100$ mJy). These four criteria are what have been used hitherto. What they do is to weed out foreground objects, and do so very effectively. Further criteria, in order to also sort out background objects, have been neglected, resulting in Bulge samples that are polluted by background PNe. Since the GBPNe are often used in the evaluation of new distance methods, and even for calibration purposes, it is very important to get a sample of Bulge PNe, that are likely to be true members, and that it is as pure from outliers as it can possibly be. To achieve this we will rework the criteria that a PN must fulfill to be treated as a member of the Bulge.

The distance to the GC is an important parameter when estimating what a typical PN in the Bulge looks like. Reid (1993) gives 8.0 kpc as the best distance, which also is the value that more recently published values cluster around, see Binney and Merrifield (1998). It is a weighted mean of a variety of methods and should be a reliable estimate.

We further assume a Bulge radius of 1.5 kpc, i.e the maximum distance a Bulge nebula will have is 9.5 kpc, and the minimum is 6.5 kpc.

5.1.1. Size limits

Fig. 1a shows the range in radii for our PNe used in the calibration. Since no attempts have been made in trying to put upper or lower limits to these radii, we believe that the range in size that those PNe represent is in a way representive for PNe in general. Upper and a lower limit on the sizes of Bulge nebulae can then be set. To do so we reject the lower and upper 8% (~ 1.5 standard deviation from the mean) of the PNe in the diagram, leading to $-1.69 < \log R < -0.50$. These limits are plotted as the two dashed vertical lines in Fig. 1a. The allowed angular size range for Bulge PNe then become, through Eq. (12),

$$0.9'' < \theta < 20'', \quad (19)$$

where maximum size is associated with minimum distance and maximum radius (i.e. $D = 6500$ pc and $\log R = -0.50$) and vice versa (i.e. $D = 9500$ pc and $\log R = -1.69$) for minimum size.

5.1.2. Flux limits

By inserting the limits of $\log R$ into our mass–radius relationship, Eq. (16), we may also set lower and upper limits to the effective mass. This leads to $-1.59 < \log M_{\mathrm{eff}} < -0.14$ (plotted as dashed horizontal lines in Fig. 1a). The reason why we use the mass–radius relation, instead of only reading these limits in Fig. 1a, is that the masses are more sensitive to errors in the derived distances than the radii ($\log M_{\mathrm{eff}} \propto 2.5 \log D$ and $\log R \propto \log D$).

Maximum radio flux is associated with minimum size (and therefore also minimum mass) and minimum distance (i.e. $\log R \sim -1.69$, $\log M_{\mathrm{eff}} \sim -1.59$, and $D \sim 6.5$ kpc), and vice versa (i.e. $\log R \sim -0.50$, $\log M_{\mathrm{eff}} \sim -0.14$, and $D \sim 9.5$ kpc) for minimum radio flux. Using again Eq. (11) and solving for the radio flux gives

$$4.2\ \mathrm{mJy} < S_{5\,\mathrm{GHz}} < 45\ \mathrm{mJy}. \quad (20)$$

In Fig. 4 we plot the new criteria (besides the coordinate critoria), Eqs. (19) and (20), for Bulge membership. They form a rectangle that restricts the values of the angular diameter and the radio flux for a PN to be treated as a Bulge nebula. These criteria will most likely also weed out a few PNe that lie in the Bulge due to their tightness. In order to get the sample as clean as possible this must be endured, at least as long as outliers are effectively deleted.

5.2. Optical or radio diameters?

The number of PNe fulfilling the coordinate criteria in the SECAT with optical diameters is 245, and with radio diameters 136. Although there is a small overlap, the radio diameters peak at considerably smaller values than the optical ones.

The discrepancies, as was also pointed out in Sect. 2, between radio and optical measurements of the angular diameter, makes it hard to decide which of the two sources to use for PNe in the Bulge. It is especially for diameters below $5''$ where the disparities are. Due to the large distances it is not possible to proceed as for our samples A and B, where sky survey plates and in many cases images from the HST Data archive were used to check on the diameters.

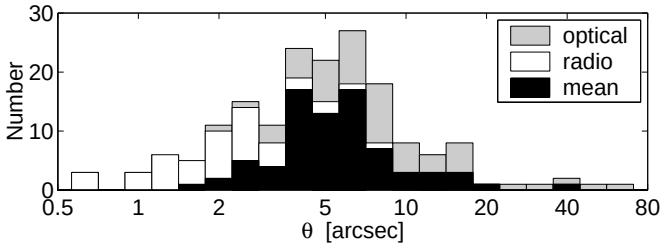

Fig. 2. Angular diameters for the 174 PNe that fulfill the coordinate criteria for Bulge membership. White parts represent PNe with radio diameters, grey PNe with optical diameters, and black PNe where a mean value of the radio and optical has been used.

To see if there are differences arising from using either optical or radio measurements of the angular diameter, a set of 61 PNe, taken from the SECAT, whose radio fluxes and angular diameters (both optical and radio) fulfill our new Bulge criteria was analyzed. Distances obtained (using our new method as well as the other methods discussed in Sect. 2) with optical diameters appear to be marginally shorter than those obtained using radio diameters. And except that radio distances seem to be more nicely distributed and slightly closer to the assumed 8 kpc distance to the GC, there are really no major differences. This makes it very difficult to judge which of the two sources for the angular sizes of PNe that is the most reliable. To minimize the risk of choosing the most erroneous value when they differ a lot, a mean value of the optical and the radio values might be to prefer. Assume that they differ by as much as 50% compared to the mean value of the two. If this difference is due to an error in just one of the values, and if the wrong one is chosen, it will lead to an error of $\sim 10\%$ in the derived distance, see Eq. (18). By instead using the mean value, the error in the derived distances due to erroneous diameters is reduced to a maximum of $\sim 5\%$ for a 50% disparity.

5.3. A sample of Bulge nebulae

To maximize the number of PNe, both optical and radio values for the angular sizes will be used, and when both are available a mean value of the two. For PNe that only have the 2 cm radio flux measured, we convert it into a corresponding 6 cm flux through the relationship $S_\nu \propto \nu^{-0.1}$. We also reject those PNe that have uncertainty flags on any of these parameters, or if the values are marked as upper/lower limits. In all this leaves 174 PNe towards the Bulge that fulfill the coordinate criteria. Fig. 2 shows the angular size distribution for these PNe. Of these there are 77 for which a mean diameter has been used. Fig. 3 shows the difference between the optical and the radio values as a function of the mean value. There are 16 that differs by more than 50%, i.e. $\sim 20\%$ of the PNe that have both radio and optical values.

For 10 of these 16 objects high-resolution optical images exist (Dopita et al., 1990; Bedding and Zijlstra, 1994 and HST image archive). In all cases, diameters determined from these images fall between the optical and the radio diameters given in SECAT, see Table 1, indicating that the use of mean values is an acceptable method. For the objects discussed here, we have however used the diameters determined from the high-resolution images. Of the remaining six objects, three fail to meet our flux criteria (Sect. 5.1.2), leaving only three objects with strongly deviating optical and radio diameters, which we choose to reject from our sample.

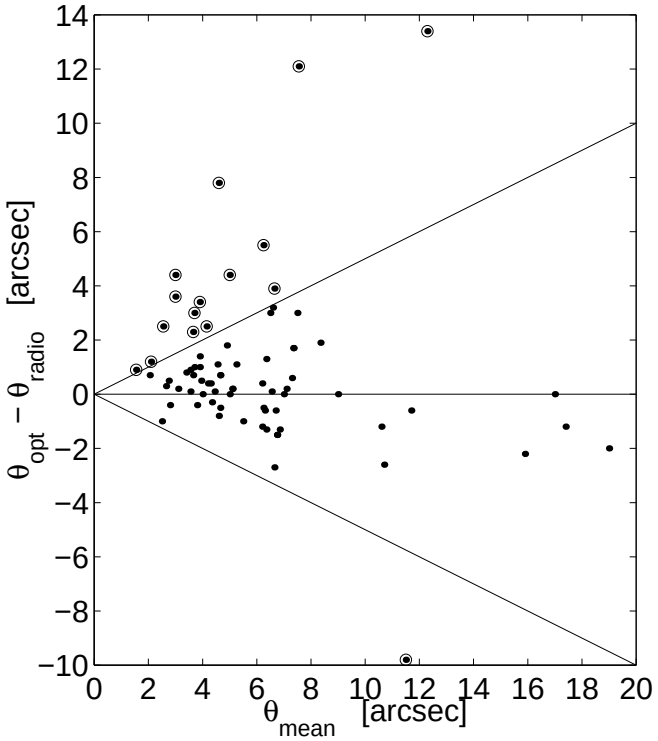

Fig. 3. In the sample of those PNe that fulfill the coordinate criteria there are 77 for which a mean value of the optical and radio diameters has been used. Here we plot the optical values minus the radio values as a function of the mean. Encircled PNe are the ones that differs by more than 50%, in all 16.

For the PNe with largely deviating diameters, the optical one is always larger than the one measured in radio. van Hoof (2000) discusses this in detail, and it seems as if the effect is real. This is due to the fact that a conversion factor has to be applied in order to achieve a true diameter from an observation at limited resolution. van Hoof shows that this conversion factor is about 10% larger for radio emission than for H_α emission. As Bedding & Zijlstra (1994) used the radio conversion factors for the optical images, they found roughly 10% larger diameters in the H_α images. In Table 1 we have reduced the 'BZ' diameters by 10%. Four of the objects then coincide with the radio diameters listed in SECAT.

Fig. 4 shows how these 174 PNe are distributed in the '$\log S_{5\,\mathrm{GHz}} - \log\theta$' plane. In the figure we also plot our new selection criteria (solid lines marked $1-4$). Those 109 PNe

Table 1. For those 10 PNe that high-resolution images are available we list here their radio and optical diameters, taken from the SECAT, as well as the diameters that we adopted after inspection of the images. The references are Dopita et al., 1990 (D90); Bedding & Zijlstra, 1994 (BZ); and the HST Archive. The diameters from BZ have been reduced by $\sim 10\%$, see discussion in the text. In all cases the adopted value fall in between the optical and the radio, indicating that using the mean value is an acceptable method.

PN G	Optical	Radio	Adopted	Ref.
002.1−04.2	4.8	1.2	2.0	HST, D90
003.5−04.6	13.6	1.5	9.0	HST
004.6+06.0	8.6	4.7	4.7	BZ
005.0+04.4	5.2	0.8	1.0	BZ
350.9+04.4	5.6	2.2	2.8	HST
355.4−02.4	7.2	2.8	4.7	BZ
355.7−03.5	2.0	1.1	1.7	BZ
357.4−03.2	5.4	2.2	2.3	BZ
358.2+04.2	5.4	2.9	2.9	BZ
359.9−04.5	4.8	2.5	3.1	D90

that lie within the rectangle are the ones that fulfill the criteria for Bulge membership. For comparison we plot the old criteria (dashed lines). We see that there are PNe with low radio fluxes and/or small angular sizes that fail to make the new demands for membership. These PNe are supposed to be background objects. Also the upper limits are tighter and weed out more (foreground) objects than before.

6. Evaluation

6.1. Local PNe – Bulge PNe

Will the same distance scale work for both local and Bulge PNe? Present models of galactic evolution as well as observations point to that the progenitor stars are very different for PNe in the various components of the Milky Way. If the mass–radius relationships of the two different populations are similar, it indicates that the origin of the relations's appearance could be fundamental. Inseparable relationships therefore demonstrates that a common distance scale should work. Fig. 5 shows this distribution for our Bulge sample, derived from Eqs. (11) and (12), assuming they all lie at a distance of 8.0 kpc. A linear regression line for this distribution is also shown (thin dotted line), as well as the adopted mass–radius relationship from Sect. 4 (solid line). By assuming that all PNe lie at 8.0 kpc we automatically introduce an error of 25% in the distances. This has the effect (as previously discussed) of steepening the observed distribution. Reducing the regression coefficients of the of the Bulge sample, in the same way as in Sect. 4, puts the Bulge mass-radius relation (strong dotted line) in closer agreement with our relationship for more local PNe.

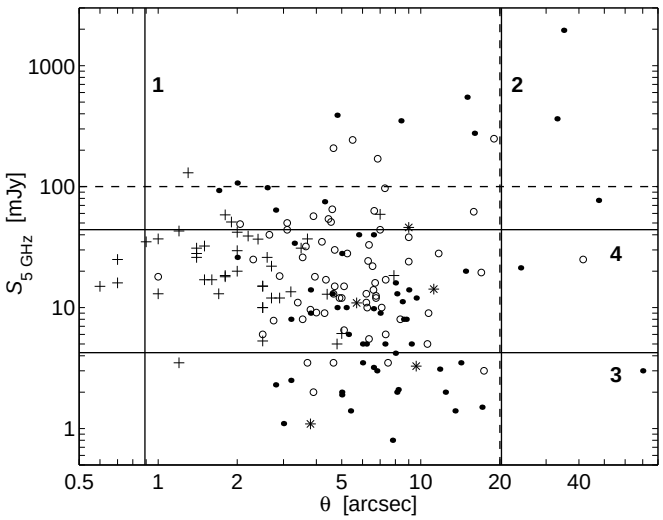

Fig. 4. Radio fluxes versus angular diameters for 174 PNe towards the Bulge located within $|l| < 10°$ and $|b| < 10°$. The different markers are: '•' – optical diameters; '○' – mean of optical and radio diameters; '+' – radio diameters; '∗' – 2 cm fluxes converted to 6 cm fluxes and optical diameters. The solid lines marked 1−4 represent the limits for our new Bulge criteria (see Sect. 5.1), where 109 are approved. For comparison we also plot the old criteria, i.e. $S_{5\,\mathrm{GHz}} < 100$ mJy and $\theta < 20''$ (dashed lines).

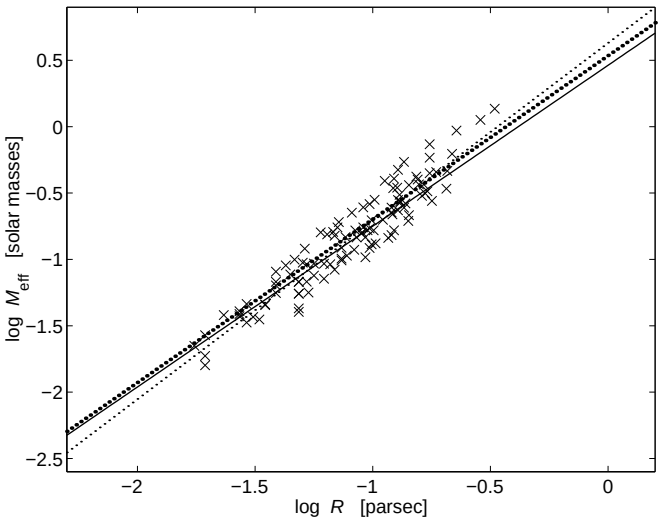

Fig. 5. Mass–radius distribution for the Bulge sample. Thin dotted line is a regression line, thick dotted line is the same regression line adjusted for errors in the distances, and the solid line is the mass–radius relationship adopted for our new distance method, see Eq. (16).

Due to the likeness, although not perfect, between the mass–radius relations for the Bulge sample and our calibration PNe, we believe that our new distance method is applicable to PNe in the Bulge as well.

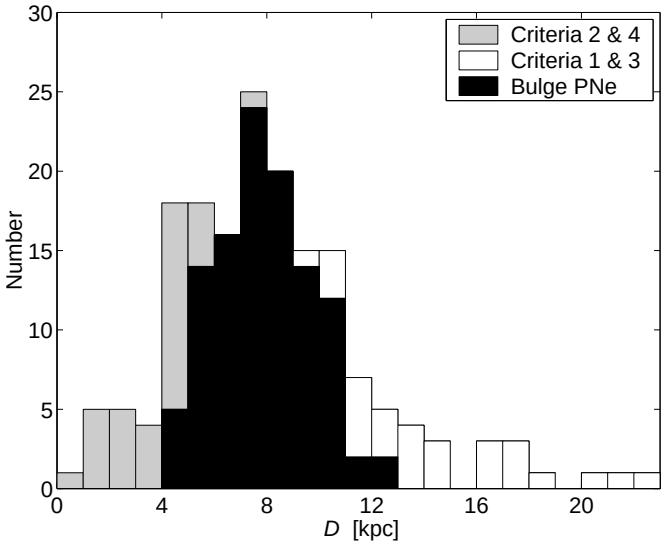

Fig. 6. The distribution of PNe towards the Bulge. White areas are background PNe that are rejected by criteria "1" and "3", and grey areas are foreground PNe sorted out by criteria "2" and "4" (see Fig. 4 and Sect. 5.1.1). The black area is the 109 PNe that remains after all criteria have been applied.

6.2. Efficiency of new Bulge criteria

Fig. 6 shows how the distribution of the PNe towards the Bulge is influenced by our new criteria. Distances are computed by our new method. Starting with 174 PNe that only fulfill the coordinate criteria, the foreground objects are reduced by criteria "2" and "4" (lines 2 and 4 in Fig. 4), and the background objects diminish through criteria "1" and "3" (lines 1 and 3 in Fig. 4). Clearly our new criteria are not only efficient in reducing foreground objects, but it also takes care of objects beyond the Bulge.

Actually the number of background PNe appears to be somewhat high. Since Bulge nebulae are mostly seen at latitudes of 2 degrees or higher, this compares to $z = 200$ pc on the near side of the Bulge and $z = 350$ pc on the far side. According to Zijlstra & Pottasch (1991) the scale height of PNe is about 250 pc. This means that there will be fewer objects causing background confusion. A plausable explanation is that the criteria also exclude those PNe for which the radio fluxes are in doubt, that is, extended PNe with a low radio flux (see Fig. 4). This effect is as important as the removal of non–Bulge members, since it certainly will influence the interpretation of the derived Bulge distributions.

Also a few PNe that, according to their distances, are members of the Bulge have been weeded out, as we suspected in Sect. 5.1. The probability of deleting a true member of the Bulge is anyway much smaller than deleting the outliers. It is important to bear in mind that the new criteria were set in order to achieve a sample free from PNe in front of and beyond the Bulge.

6.3. New method vs. Old methods - using Bulge PNe

A way to test if a distance method is consistent is to try it on two different sets of PNe: one where they are supposed to be optically thin, and one where they are supposed to be optically thick. The mass limit when a PN becomes optically thin is somewhat uncertain but should approximately be when the ionized envelope reaches a radius of ~ 0.2 pc. For GBPNe, which are supposed to have an average distance of 8 kpc, this radius compares to an angular diameter of $\sim 5''$, which is by coincidence where our sample of Bulge nebulae peaks, see Fig. 2. Splitting the sample in two, one with angular diameters larger than or equal to $4.6''$ and one with angular diameters smaller than $4.6''$ gives two samples consisting of 56 and 53 PNe respectively.

What kind of differences can we expect from a such division? If we go back to the classical Shklovsky method which assumes a constant mass (usually 0.2 $M_\odot$) for all PNe, both large and small, we might see how this method overestimates the masses for small PNe, and therefore also their distances. Larger PNe, on the other side, which actually seem to cluster around an ionized mass of ~ 0.2 $M_\odot$, should have distances with a quite high degree of accuracy. If our new method, as well as the other previously discussed methods, is to be used as a good distance estimator for PNe, the difference between the distance distributions for the small and the large nebulae should preferably be small. It is important to point out that it is not very likely that they should be identical, due to the difficulty of achieving a statistically complete non–biased sample of PNe in the Bulge.

Fig. 7 shows the distance distributions of the 109 Bulge PNe, divided into the large and small samples, and Table 2 shows some statistics.

6.3.1. Large PNe

Although one might expect the distribution of larger nebulae to peak at a somewhat shorter distance than the conventional 8 kpc to the GC, the large discrepancies for CKS, VdSZ, Z95 and SB96, where more than 75% of the

Table 2. Statistics for the distance distributions of the different methods for the Bulge sample. $D_{0.5}$ is the median value, $\langle D \rangle$ the mean, and σ_D the standard deviation. 'S' means small, 'L' large, 'A' all, and they are 53, 56 and 109 respectively.

	$D_{0.5}$ [kpc]			$\langle D \rangle$ [kpc]			σ_D [kpc]		
	A	S	L	A	S	L	A	S	L
This Work	7.8	8.1	7.5	7.9	8.2	7.6	1.8	1.8	1.8
SB96	7.6	8.8	6.7	7.7	8.7	6.6	1.9	1.7	1.4
Z95	7.8	8.3	7.2	7.8	8.3	7.2	1.8	1.7	1.7
VdSZ	7.2	8.0	6.7	7.3	7.9	6.7	1.7	1.6	1.5
CKS	6.6	6.4	6.8	7.0	7.1	6.9	2.1	2.7	1.5
Shklovsky	9.9	13.1	7.8	11.1	13.8	8.6	4.8	3.6	4.4

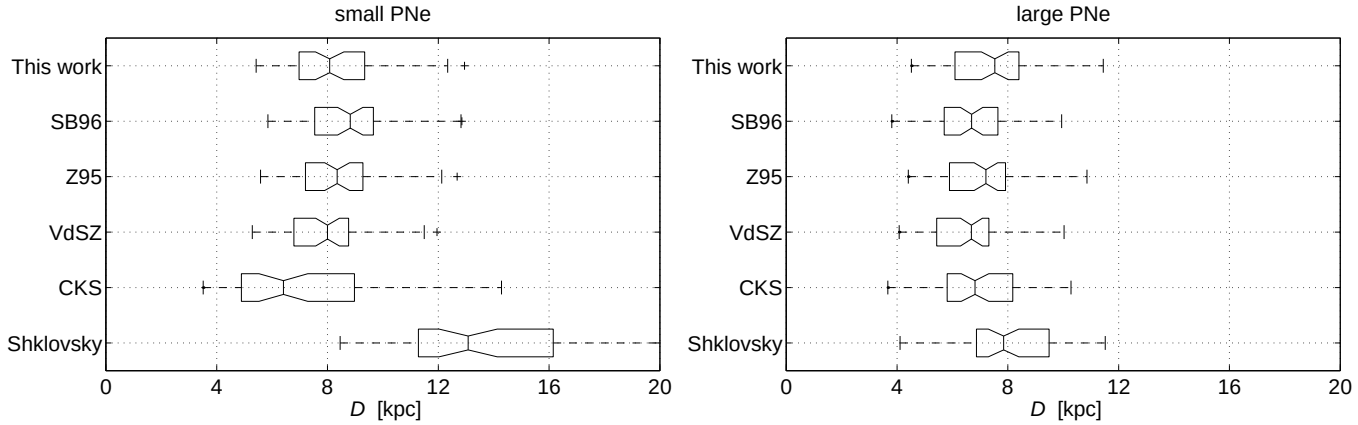

Fig. 7. Comparison of our new method with the old methods for PNe that fulfill the new Bulge criteria. CKS, VdSZ, Z95 and SB96 distances were derived from Eqs. (5), (7), (8) and (10), and the Shklovsky distances from Eq. (3). The distributions are shown as box–plots where the boxes have lines at the lower quartile, median and upper quartile values. The whiskers are lines extending from each end of the box to show the extent of the rest of the data. Outliers are marked with plus signs and are defined as those PNe whose distance is more than 1.5 times the interquartile range away from the top or bottom of the box. The notches in the box are graphic confidence intervals about the median of the sample. The number of small PNe is 53, and large PNe is 56 in all samples.

samples are located on this side of the GC, are rather unexpected. Especially for VdSZ, that used GBPNe in their calibration, the result may be a consequence of the neglection of the background objects in their Bulge sample. Our method has on the other side a distribution that is more centered around the GC, although not perfectly.

One reason to why the distributions tend to shorter distances is probably an effect of the non–completeness of the Bulge sample. The surface brightness of a PN, which is a distance independent parameter, is on average lower for a large nebula. Due to extinction in the Galaxy, PNe beyond the GC are more likely to fall below the limit of detectability, compared to those on this side. This will show as an increase of PNe on this side of the GC relatively PNe beyond the GC.

A second possible explanation, as mentioned in Sect. 6.2, is that the Bulge criteria also exclude those PNe for which the radio fluxes are in doubt.

Another possible reason is that the large nebulae diameters are dominated by optical determinations, see Fig. 2. As we saw in Sect. 5.3 from high-resolution images of some of the PNe that have both optical and radio diameters, the "correct" values should be somewhere in between the radio and the optical. This means that optical values are on average slightly too large and the radio values on average too small. This has the effect of placing large PNe at too short distances and small PNe at too long distances. How large these effects are on the distance distribution of the large PNe is obscure, but we believe that the discrepancies that the old methods show are too large.

6.3.2. Small PNe

In practice all methods (except CKS and Shklovsky) show a distribution that is well centered around the GC for the small PNe. A general trend is also that the small PNe give distance distributions that peaks at larger distances than for the large PNe. The causes for this are almost certainly of the same types as discussed in Sect. 6.3.1.

6.3.3. Whole sample

It is striking to see how well our method coincides with the method by Z95 when both small and large PNe are counted in. One could maybe draw the conclusion that this is an effect of the dominance of PNe from Zhang (1993) in our calibration sample B. But if the calibration from Sect. 4 is repeated with only PNe from this sample, the regression coefficients, not corrected for the increased steepening, become

$$\alpha = 1.55 \pm 0.04, \qquad \beta = 0.86 \pm 0.05. \tag{21}$$

i.e. quite different from the ones we achieved. Also, since these PNe were down–weighted by 0.5 with respect to those in sample A, we do not believe that our method is too similar to Z95 although the distribution (Table 2) indicate that they are. Instead we interpret the likeness between the two methods as a confirmation of the statistical methods as distance indicators, although they differ in appearance, see Eqs. (8) and (18).

Our method and Z95 are the ones that center nearest to 8.0 kpc. The other methods give distances considerably below this well-established distance to the GC. Since we do not know the completeness of the Bulge sample, it is not possible to say which of the methods that is the best. One thing there is no doubts about though, is that the CKS and the Shklovsky methods give distances that are far too short and too long respectively.

6.4. The legality of statistical distances

Table 2 shows the spread of distances to bulge nebulae found using the different methods discussed. All recent investigations have values around 1.8 kpc. Assuming that the probable error in distance for one nebula is around 15%, and that the Bulge has a radius of 1.5 kpc, we would in fact expect a spread of around 1.9 kpc. Since our strong membership criteria certainly exclude some true Bulge nebulae from our sample, the errors are probably somewhat larger, but most probably less than 30% as also indicated from our calibration sample (Sect. 4.1).

This is comparable with errors expected from several "individual" distance determination methods. For example, Mendez et al. (1988) estimate that errors in distances from high–resolution spectroscopic determinations of effective temperatures and surface gravities of central stars of PNe amounts to $\sim$ 25%. The method using resolved binary components also involves errors in absolute magnitude and reddening corrections of at least 0.3 mag. (Ciardullo et al., 1999). This corresponds to errors in distance of around 15%. A more realistic(?) estimate of a total error approaching 0.5 mag. correspond to a 25% error in distance. Only a few objects have trigonometric parallaxes determined with errors smaller than 30%. Other proposed methods have also comparable or higher uncertainties.

From Fig. 7 and Table 2 it is difficult to objectively decide which of the discussed methods that give the best result for the Bulge test sample. The original Shklovsky method and the CKS relation are obviously inferior to the other methods. VdSZ fail to give the expected distance to the Bulge, while SB96 gives a relatively large difference between the two subsamples. Z95 and the present investigation give practically equally good results for the Bulge nebulae.

Due to the uncertainty of the appearance of the mass–radius relationship for very compact and very extended PNe, a warning may be in place to use the statistical methods for these objects. As can be seen from Fig. 1 the PNe within the central rectangle are well represented by a linear function, and for those we expect our method to give distances with high accuracy. Leaving out extreme PNe is not a large limitation on the usefulness of the method since the majority of PNe are in an evolutionary stage such that they fall into the central group.

7. Conclusions

We have recalibrated the correlation between the ionized mass and the nebular radius for Galactic PNe to enable an analyze of the distances that statistical methods produce. For the first time the mass–radius relationship has been compensated for the steepening and shift, which is the inevitable effect that errors in the distances have on the distribution of the nebulae in the '$\log M$–$\log R$' plane. In order to compare our new method with other statistical distance methods we reworked the criteria for Bulge membership. The old criteria did not pay attention to the problem of background objects, leading to Bulge samples that were polluted by PNe at long distances. Our new criteria are quite tight, meaning that they almost certainly also weed out true members of the Bulge. Since they were taken out in order to produce a sample that is as clean from outliers as possible, this is an unavoidable effect.

Applying the new criteria on PNe from the SECAT we derived a sample of 109 nebulae that are likely to be located within the Bulge. Using this sample, and calculating distances using our new method as well as the old methods we show that our method gives distances with a high degree of accuracy, fully comparable to individual distance determinations. Also noticed is that all the older statistical methods give shorter distances.

We also divided the Bulge sample into two samples, one with optically thick PNe, and one with optically thin PNe. This was done in order to check on the consistency of the methods. All methods (except CKS) give distance distributions at longer distances for the small (optically thick) PNe compared to the larger ones. Also all methods, except our, give distances to the large nebulae that are too short. We believe that this is partly due to the incompleteness of the Bulge sample. It is not likely, though, that it is completely responsible for the large discrepancy from the 8 kpc distance to the GC that the old methods show for large PNe. Small PNe show in general a well centered distance distribution around the GC.

With this work we believe that the method of determining distances to PNe in a statistical way has been settled. The long distance scales of VdSZ and Z95 are in a way confirmed, although small differences persist. The way VdSZ selected their Bulge sample, used for calibration, is a reason to why differences are found. Older, and shorter, distance scales, such as the one by Daub (recalibrated by CKS) are basically outdated.

Acknowledgements. We wish to thank our referee Dr. Albert Zijlstra for his remarks which allowed us to see more clearly, improving the analysis and text of the paper. This investigation is partly based on observations made with the NASA/ESA Hubble Space Telescope, obtained from the data archive at the Space Telescope Institute. STScI is operated by the association of Universities for Research in Astronomy, Inc. under the NASA contract NAS 5-26555.

References

Aaquist O.B. and Kwok S., 1990, A&AS, 84, 229
Aaquist O.B. and Kwok S., 1991, ApJ, 378, 599
Acker A., 1978, A&AS, 33, 367
Acker A., Ochsenbein F., Stenholm B., Tylenda R. and Marcout J., 1992, The Strasbourg-ESO Catalogue of Galactic Planetary Nebulae, ESO
Acker A., Fresnau A., Pottasch S.R. and Jasniewicz G., 1998, A&A, 337, 253
Basart J.P. and Daub C.T., 1987, ApJ, 317, 412
Bedding T.R. and Zijlstra A.A., 1994, A&A, 283, 955
Binney J. and Merrifield M., 1998, Galactic Astronomy, Princeton University Press, Princeton, New Jersey

Birkinshaw M., Downes A.J.B. and Pooley G.G., 1981, Observatory, 101, 120
Bond H.E. and Ciardullo R., 1999, PASP, 111, 217
Bässgen M., Diesch C. and Grewing M., 1995, 297, 828
Cahn J.H. and Kaler J.B., 1971, ApJS, 22, 319
Cahn J.H., Kaler J.B. and Stanghellini L., 1992, A&AS, 94, 399
Christianto H. and Seaquist E.R., 1998, AJ, 115, 2466
Chu Y., Jacoby G.H. and Arendt R., 1987, ApJS, 64, 529
Ciardullo R., Bond H.E., Sipior M.S., Fullton L.K., Zhang C.Y. and Schaefer K.G., 1999, AJ, 118, 488
Costero R., Tapia M., Mendez R.H., Echevarria J., Roth M., Quintero A. and Barral J.F., 1986, Rev. Mex. Astron. Astrofis., 13, 149
Daub C.T., 1982, ApJ, 260, 612
Dopita M.A., Henry J.P., Tuohy I.R., Webster B.L., Roberts E.H., Byun Y.-I., Cowie L.L. and Songaila A., 1990, ApJ, 365, 640
Gathier R., Pottasch S.R. and Goss W.M., 1983a, A&A, 127, 320
Gathier R., Pottasch S.R., Goss W.M. and Gorkom J.H., 1983b, A&A, 128, 325
Gathier R., Pottasch S.R. and Pel J.W., 1986a, A&A, 157, 171
Gathier R., Pottasch S.R. and Goss W.M., 1986b, A&A, 157, 191
Gurzadyan G.A., 1970, Planetary Nebulae, D. Reidel Publishing Company, Dordrecht, Holland
Gutiérrez-Moreno A., Anguita C., Loyola P. and Moreno H., 1999, PASP, 111, 1163
Hajian A.R., Terzian Y. and Bignell C., 1993, AJ, 106, 1965
Hajian A.R., Terzian Y. and Bignell C., 1995, AJ, 109, 2600
Hajian A.R., Frank A., Balick B. and Terzian Y., 1997, ApJ, 477, 226
Harrington R.S. and Dahn C.C., 1980, AJ, 85, 454
Harris H.C., Dahn C.C., Monet D.G. and Pier J.R., 1997, IAUS 180 Planetary Nebulae, H.J. Habing and H.J.G.L.M. Lamers (eds.), 40
Higgs L.A., 1971, MNRAS, 153, 315
Hua C.T. and Kwok S., 1999, A&AS, 138, 275
Huemer G. and Weinberger R., 1988, A&AS, 72, 383
Isaacman R., 1984, MNRAS, 208, 399
Jacoby G.H., 1988, ApJ, 333, 193
Kaler J.B. and Lutz J.H., 1985, PASP, 97, 700
Kaler J.B., Jing-Er M. and Pottasch S.R., 1985, ApJ, 288, 305
Kohoutek L., 1995, A&AS, 113, 107
Lucke P.B., 1978, A&A, 64, 367
Lutz J.H., 1973, ApJ, 181, 135
Maciel W., 1996, Rev. Mex. Astron. Astrofis. Ser. de Conf., 4, 83
Maciel W.J. and Cazetta J.O., 1997, Ap&SS, 249, 341
Maciel W.J. and Pottasch S.R., 1980, A&A, 88, 1
Martin W., 1994, A&A, 281, 526
Masson C.R., 1986, ApJ, 301, L27
Masson C.R., 1989, ApJ, 336, 294
Meatheringham S.J., Wood P.R. and Faulkner D.J., 1988, ApJ, 334, 862
Mendez R.H. and Niemela V.S., 1981, ApJ, 250, 240
Méndez R.H., Kudritzki R.P., Herrero A., Husfeld D. and Groth H.G., 1988, A&A, 190, 113
Méndez R.H., Kudritzki R.P. and Herrero A., 1992, A&A, 260, 329
Milne D.K., 1979, A&AS, 36, 227
Milne D.K. and Aller L.H., 1975, A&A, 38, 183
Milne D.K. and Aller L.H., 1982, A&AS, 50, 209
Moreno H., Lasker B.M., Gutiérrez-Moreno A. and Torres C., 1988, PASP, 100, 604
Napiwotzki R. and Schönberner D.,1995, A&A, 301, 545
Perek L. and Kohoutek L., 1967, Catalogue of galactic planetary nebulae, Publication House Czechoslovak Academy of Sciences, Prague
Phillips J.P. and Mampaso A., 1988, A&A, 190, 237
Pier J.R., Harris H.C., Dahn C.C. and Monet D.G., 1993, IAUS 155, Planetary Nebulae, Weinberger R. and Acker A. (eds.), 175
Pollacco D.L. and Ramsay G., 1992, MNRAS, 254, 228
Pottasch S.R., 1980, A&A, 89, 336
Pottasch S.R., 1983, IAUS 103, Planetary Nebulae, D.R. Flower (ed.), 391
Pottasch S.R., 1984, Planetary Nebulae, D. Reidel Publishing Company, Dordrecht, Holland
Pottasch S.R., 1987, Planetary and Proto-Planetary Nebulae: from IRAS to ISO, Proceedings of the Frascati workshop, Volcano Island sep. 8-12, 1986, Martinez P. (ed.), 79
Pottasch S.R., 1996, A&A, 307, 561
Pottasch S.R. and Zijlstra A.A., 1992, A&A, 256, 251
Pottasch S.R. and Zijlstra A.A., 1994, A&A, 289, 261
Pottasch S.R., Goss W.M., Arnal E.M. and Gathier R., 1982, A&A, 106, 229
Pottasch S.R., Bignell C., Olling R. and Zijlstra A.A., 1988, A&A, 205, 248
Press W.H., Teukolsky S.A., Vetterling W.T. and Flannery B.P., 1997, Numerical Recipes in C – The Art of Scientific Computing, 2nd edition, Cambridge University Press
Purton C.R., Feldman P.A., Marsh K.A., Allen D.A. and Wright A.E., 1982, MNRAS, 198, 321
Ratag M.A. and Pottasch S.R., 1991, A&AS, 91, 481
Reid M.J., 1993, ARA&A, 31, 345
Sabbadin F., 1986, A&AS, 64, 579
Saurer W., 1997, A&A, 328, 641
Saurer W., 1998, MNRAS, 299, 51
Schneider S.E. and Buckley D., 1996, ApJ, 459, 606
Seaquist E.R. and Davis L.E., 1983, ApJ, 274, 659
Shklovsky I.S., 1956, AZh, 33, 315
Stasińska G., Tylenda R., Acker A. and Stenholm B., 1991, A&A, 247, 173
Tylenda R., Acker A., Stenholm B. and Köppen J., 1992, A&AS, 95, 337
Van de Steene G.C. and Zijlstra A.A., 1995, A&A, 293, 541
van Hoof P.A.M., 2000, MNRAS, 314, 99
Walsh J.R., Walton N.A. and Pottasch S.R., 1993, IAUS 155, Planetary Nebulae, Weinberger R. and Acker A. (eds), 390
Zhang C.Y., 1993, ApJ, 410, 239
Zhang C.Y., 1995, ApJS, 98, 659
Zijlstra A.A. and Pottasch S.R., 1991, A&A, 243, 478
Zijlstra A.A., Pottasch S.R. and Bignell C., 1989, A&AS, 79, 329

Appendix

Table A. Sample A: 41 PNe with at least three individual distance determinations. For references of the adopted values on D, θ and $S_{5\,\mathrm{GHz}}$, see Table C.

PN G	Name	D [pc]	N	$\Delta D/D$	θ [$''$]	$S_{5\,\mathrm{GHz}}$ [mJy]	M_{eff} [$M_{\odot}$]	R [pc]
002.4+05.8	NGC 6369	1490	4	0.15	35.0	1958	0.61	0.13
009.4−05.0	NGC 6629	1956	8	0.10	16.0	276	0.14	0.076
010.1+00.7	NGC 6537	2110	4	0.11	10.0	628	0.13	0.051
010.8−01.8	NGC 6578	2350	4	0.17	8.5	164	0.066	0.048
011.7−00.6	NGC 6567	1271	11	0.06	7.0	167	0.011	0.022
023.9−02.3	M1-59	1293	3	0.11	6.5	130	0.0088	0.020
029.2−05.9	NGC 6751	1961	4	0.19	22.0	62	0.11	0.10
033.1−06.3	NGC 6772	1260	4	0.02	65.0	88	0.21	0.20
033.8−02.6	NGC 6741	1477	6	0.13	8.0	194	0.020	0.029
036.1−57.1	NGC 7293	216	9	0.11	660.0	1292	0.32	0.35
037.7−34.5	NGC 7009	1076	10	0.17	28.5	736	0.12	0.074
041.8−02.9	NGC 6781	1567	3	0.02	108.0	340	1.6	0.41
043.1+37.7	NGC 6210	1630	4	0.13	30.0	258	0.22	0.12
045.4−02.7	Vy 2-2	3800	3	0.11	1.0	264	0.011	0.0092
045.7−04.5	NGC 6804	1525	4	0.12	35.0	136	0.17	0.13
046.4−04.1	NGC 6803	1733	6	0.18	5.5	109	0.013	0.023
069.4−02.6	NGC 6894	1428	5	0.11	42.0	61	0.13	0.15
084.9−03.4	NGC 7027	1045	8	0.13	14.0	6130	0.11	0.036
088.7−01.6	NGC 7048	1725	4	0.15	61.0	37	0.28	0.26
093.4+05.4	NGC 7008	883	6	0.14	86.0	217	0.21	0.18
118.8−74.7	NGC 246	496	10	0.05	245.0	262	0.26	0.29
197.8+17.3	NGC 2392	1176	10	0.19	19.5	262	0.051	0.056
205.1+14.2	A21	513	6	0.09	550.0	390	1.2	0.68
215.6+03.6	NGC 2346	904	14	0.09	52.0	86	0.066	0.11
234.8+02.4	NGC 2440	1753	12	0.14	20.0	397	0.18	0.085
243.3−01.0	NGC 2452	3217	7	0.08	19.0	58	0.29	0.15
261.0+32.0	NGC 3242	901	11	0.18	25.0	860	0.069	0.055
265.7+04.1	NGC 2792	2507	6	0.07	13.0	115	0.12	0.079
272.1+12.3	NGC 3132	644	9	0.08	30.0	228	0.020	0.047
278.1−05.9	NGC 2867	1908	7	0.14	14.0	274	0.11	0.065
286.3−04.8	NGC 3211	2833	4	0.14	16.0	86	0.20	0.11
294.1+43.6	NGC 4361	1442	6	0.11	63.0	218	0.45	0.22
294.6+04.7	NGC 3918	1537	6	0.15	19.0	856	0.17	0.071
298.3−04.8	NGC 4071	1133	3	0.16	63.0	26	0.085	0.17
307.2−03.4	NGC 5189	1266	5	0.15	140.0	462	1.6	0.43
309.1−04.3	NGC 5315	2564	5	0.14	6.0	444	0.080	0.037
316.1+08.4	He2-108	4900	3	0.15	11.0	40	0.30	0.13
320.1−09.6	He2-138	2775	4	0.11	7.0	84	0.053	0.047
341.8+05.4	NGC 6153	1668	4	0.03	24.0	550	0.24	0.097
350.9+04.4	H2-1	4167	3	0.07	2.8	64	0.032	0.028
358.9−00.7	M1-26	1733	6	0.11	4.8	389	0.020	0.020

Table B. Sample B: 32 PNe with only two individual distance determinations. For references of the adopted values on D, θ and $S_{5\,\mathrm{GHz}}$, see Table C.

PN G	Name	D [pc]	N	$\Delta D/D$	θ [$''$]	$S_{5\,\mathrm{GHz}}$ [mJy]	M_{eff} [$M_{\odot}$]	R [pc]
000.3+12.2	IC 4634	4900	2	0.10	8.4	123	0.35	0.10
002.0−13.4	IC 4776	7350	2	0.14	7.5	69	0.61	0.13
002.1−04.2	H 1-54	11650	2	0.02	2.0	26	0.16	0.057
002.4−03.7	M 1-38	6400	2	0.05	3.3	34	0.088	0.051
003.7−04.6	M 2-30	12100	2	0.15	9.0	14	1.3	0.26
005.8−06.1	NGC 6620	4400	2	0.02	8.0	16	0.090	0.085
008.0+03.9	NGC 6445	2250	2	0.11	33.0	364	0.67	0.18
008.3−07.3	NGC 6644	3000	2	0.07	2.6	98	0.016	0.019
025.8−17.9	NGC 6818	2230	2	0.01	30.0	291	0.51	0.16
065.0−27.3	Ps 1	11550	2	0.17	2.4	5	0.092	0.067
074.5+02.1	NGC 6881	6250	2	0.02	2.6	121	0.11	0.039
093.3−02.4	M 1-79	2350	2	0.15	33.0	19	0.17	0.19
107.6−13.3	Vy 2- 3	11350	2	0.07	4.5	3	0.18	0.12
111.8−02.8	Hb 12	5750	2	0.15	1.0	367	0.037	0.014
118.0−08.6	Vy 1- 1	6650	2	0.04	6.0	20	0.18	0.097
161.2−14.8	IC 2003	9750	2	0.04	9.0	47	1.3	0.21
190.3−17.7	J 320	6300	2	0.13	9.0	28	0.35	0.14
238.0+34.8	A 33	1210	2	0.04	280.0	39	1.1	0.82
291.6−04.8	IC 2621	4750	2	0.01	5.0	195	0.19	0.058
296.3−03.0	He 2- 73	6500	2	0.03	4.0	72	0.18	0.063
312.3+10.5	NGC 5307	2470	2	0.05	16.0	92	0.14	0.096
321.3+02.8	He 2-115	4000	2	0.05	3.0	132	0.047	0.029
323.9+02.4	He 2-123	6150	2	0.01	4.6	84	0.21	0.069
325.8−12.8	He2-182	5350	2	0.18	2.5	66	0.052	0.032
326.0−06.5	He2-151	6800	2	0.01	1.0	7	0.0078	0.017
327.1−02.2	He 2-142	3850	2	0.04	3.6	70	0.041	0.034
329.0+01.9	Sp 1	1450	2	0.10	72.0	76	0.33	0.25
331.3+16.8	NGC 5873	9200	2	0.18	7.0	45	0.78	0.16
331.4−03.5	He2-162	4000	2	0.08	5.0	23	0.042	0.049
355.1−06.9	M 3-21	8500	2	0.07	5.0	28	0.30	0.10
355.7−03.5	H 1-35	8050	2	0.07	1.7	93	0.096	0.033
355.9−04.2	M 1-30	7950	2	0.01	3.5	31	0.16	0.067

Table C. References for the distances (D), radio fluxes ($S_{5\,\mathrm{GHz}}$) and the diameters (θ) in Tables A and B.

Distances:

(1) Acker (1978), (2) Acker et al. (1998), (3) Bond and Ciardullo (1999), (4) Bässgen et al. (1995), (5) Christianto and Seaquist (1998), (6) Ciardullo et al. (1999), (7) Costero et al. (1986), (8) Gathier et al. (1986a), (9) Gathier et al. (1986b), (10) Gurzadyan (1970) (11) Gutiérrez-Moreno et al. (1999), (12) Hajian et al. (1993), (13) Hajian et al. (1995), (14) Hajian et al. (1997), (15) Harrington and Dahn (1980), (16) Harris et al. (1997), (17) Huemer and Weinberger (1988), (18) Jacoby (1988), (19) Kaler and Lutz (1985), (20) Kaler et al. (1985), (21) Kohoutek (1995), (22) Lutz (1973), (23) Maciel (1996), (24) Maciel and Cazetta (1997), (25) Maciel and Pottasch (1980), (26) Martin (1994), (27) Masson (1986), (28) Masson (1989), (29) Meatheringham et al. (1988), (30) Mendez and Niemela (1981), (31) Mendez et al. (1992), (32) Napiwotzki and Schönberner (1995), (33) Pier et al. (1993), (34) Pollacco and Ramsay (1992), (35) Pottasch (1980), (36) Pottasch (1983), (37) Pottasch (1984), (38) Pottasch (1987), (39) Pottasch (1996), (40) Pottasch et al. (1982), (41) Sabbadin (1986), (42) Saurer (1997), (43) Saurer (1998), (44) Zhang (1993), (45) Walsh et al. (1993).

Fluxes:

(46) Aaquist and Kwok (1990), (47) Basart and Daub (1987), (48) Birkinshaw et al. (1981), (49) Gathier et al. (1983a), (50) Gathier et al. (1983b), (51) Higgs (1971), (52) Isaacman (1984), (53) Milne and Aller (1975), (54) Milne and Aller (1982), (55) Phillips and Mampaso (1988), (56) Pottasch and Zijlstra (1994), (57) Purton et al. (1982), (58) Ratag and Pottasch (1991), (59) Zijlstra et al. (1989).

Diameters:

(60) Aaquist and Kwok (1990), (61) Bedding and Zijlstra (1994), (62) Cahn and Kaler (1971), (63) Chu et al. (1987), (64) Dopita et al. (1990), (65) Gathier et al. (1983b), (66) HST Archive broad band image, (67) HST Archive H-alpha image, (68) HST Archive [NII] image, (69) Hua and Kwok (1999), (70) Mendez et al. (1988), (71) Milne and Aller (1975), (72) Moreno et al. (1988), (73) Perek and Kohoutek (1967), (74) Seaquist and Davies (1983), (75) Zijlstra et al. (1989).

PN G	D-ref	S-ref	θ-ref	PN G	D-ref	S-ref	θ-ref
Sample A				320.1−09.6	24,31,44	53,54	62,67
002.4+05.8	9,29,36,44	53,54	63,66	341.8+05.4	29,36,41,44	53,54	62,63
009.4−05.0	9,14,24,29,31,36,41,44	53,54	63,66	350.9+04.4	24,31,44	53,54,59	67
010.1+00.7	1,9,29,36	52,53,54,55	67	358.9−00.7	1,24,31,41,44	46,53,54	62,67
010.8−01.8	9,36,41,44	53,54	63,66				
011.7−00.6	1,8,9,25,35,36,37,41,44	53,54	63	**Sample B**			
023.9−02.3	1,35	52,53,54,59	67	000.3+12.2	44	46,53,54,55,58	62,67
029.2−05.9	1,14,36,44	53,54	63,68	002.0−13.4	44	53,54,55	62,63
033.1−06.3	1,29,36,41	53,54,59	62	002.1−04.2	44	50,54	64,67
033.8−02.6	1,19,36,41,44	52,53,54,59	63,68	002.4−03.7	44	50,54	65,73
036.1−57.1	15,16,24,31,35,37,39,44	53	71,75	003.7−04.6	44	54,59	72
037.7−34.5	1,20,23,24,25,29,31,35,36,44	53,54	63,68	005.8−06.1	44	53,54,55,56	62,72
041.8−02.9	1,36,41	53,54,59	63,66	008.0+03.9	36,41	53,54	62
043.1+37.7	13,25,44	53,54	63,67	008.3−07.3	25,44	50.55	62,63
045.4−02.7	5,44	57	67,74	025.8−17.9	10,29	53,54	67
045.7−04.5	1,36,41	53,54	63,66	065.0−27.3	25,41	48,49,53,54	67
046.4−04.1	1,9,35,36,41	53,54,55	62,63	074.5+02.1	44	46,55	60,67
069.4−02.6	1,19,22,36,41	59	63,66	093.3−02.4	42,43	59	62
084.9−03.4	12,18,27,28,37,39,40,41	59	63,67	107.6−13.3	44	59	62,67,75
088.7−01.6	1,17,41	59	63	111.8−02.8	44	57	60,67
093.4+05.4	1,6,35,36,41	59	63,66	118.0−08.6	44	46,55	60
118.8−74.7	2,3,35,36,39,45	53,54	63	161.2−14.8	44	46,55	60,62,63
197.8+17.3	10,13,23,24,25,31,35,36,41,44	53,54	63,67	190.3−17.7	44	46,53,54,55	67
205.1+14.2	11,16,32,33,39	53,54	69	238.0+34.8	6,39	53,54	69
215.6+03.6	1,7,8,21,29,30,35,36,37,39	53	62,67	291.6−04.8	44	53,54	63
234.8+02.4	1,4,8,9,10,29,34,36,37,38,44	53,54,59	66,75	296.3−03.0	44	53,54	62
243.3−01.0	1,8,29,35,36,37,44	53,54	62,66	312.3+10.5	29,44	53,54	63,66
261.0+32.0	10,13,20,24,25,31,35,36,41,44	53,54	63,67	321.3+02.8	44	53,54	62,67
265.7+04.1	1,8,29,36,37,44	53,54	63,66	323.9+02.4	44	53,54	62
272.1+12.3	6,8,29,35,36,39,41	53,54	63,67	325.8−12.8	24,31	53,54	67
278.1−05.9	1,14,29,36,41,44	53,54	62,66	326.0−06.5	24,31	54	67
286.3−04.8	8,36,29,44	53,54	62	327.1−02.2	44	53,54	62,67
294.1+43.6	24,29,31,37,39,44	53,54	63	329.0+01.9	1,41	53,54	62
294.6+04.7	1,8,29,36,41,44	53,54	62,66	331.3+16.8	44	53,54,55	62
298.3−04.8	1,41,44	53,54	62	331.4−03.5	44	53,54	70